Combined DFT and DEMS investigation of the effect of dopants in secondary zincair batteries

Lysgaard, Steen; Christensen, Mathias K.; Hansen, Heine A.; García Lastra, Juan Maria; Norby, Poul; Vegge, Tejs

Published in:
ChemSusChem (Print)

Link to article, DOI:
10.1002/cssc.201800225

Publication date:
2018

Document Version
Peer reviewed version

Combined DFT and DEMS investigation of the effect of dopants in secondary zinc-air batteries

Steen Lysgaard*, Mathias K. Christensen, Heine A. Hansen, Juan Maria García Lastra, Poul Norby and Tejs Vegge*[a]

[a] Dr. S. Lysgaard, M. K. Christensen, Assoc. Prof. H. A. Hansen, Assoc. Prof. J. M. G. Lastra, Prof. P. Norby, Prof. T. Vegge

Department of Energy Conversion and Storage

Technical University of Denmark, 2800 Kgs. Lyngby (Denmark)

Homepage: http://www.asc.energy.dtu.dk/

Email: S. Lysgaard: stly@dtu.dk, T. Vegge: teve@dtu.dk

ORCID: S. Lysgaard: 0000-0002-2032-8949

ORCID: T. Vegge: 0000-0002-1484-0284

Abstract

Zinc-air batteries offer the potential of low cost energy storage with high specific energy, but at present secondary Zn-air batteries suffer from poor cyclability. To develop economically viable secondary Zn-air batteries, several properties need to be improved: choking of the cathode, catalyzing the oxygen evolution and reduction reactions, limiting dendrite formation and suppressing the hydrogen evolution reaction (HER). Understanding and alleviating HER at the negative electrode in a secondary Zn-air battery is a substantial challenge, where it is necessary to combine computational and experimental research.

Here, we combine Differential Electrochemical Mass Spectrometry (DEMS) and density functional theory (DFT) calculations to investigate the fundamental role and stability over cycling of selected beneficial additives, i.e. In and Bi, and Ag as a potentially unfavorable additive. We show that both In and Bi have the desired property for a secondary battery that upon recharging, they will remain in the surface, thereby retaining the beneficial effects on Zn dissolution and suppression of HER. This is confirmed by DEMS, where we observe that In lowers HER and Bi affects the discharge potential beneficially, compared to a battery without additives. Using a simple procedure based on adsorption energies calculated with DFT, we find that Ag suppress OH adsorption but, unlike In and Bi, does not hinder HER. Finally, it is shown that mixing In and Bi is beneficial compared to the additives by themselves, as it improves the electrochemical performance and cyclic stability of the secondary Zn-air battery.

Introduction

Today's challenge of transforming society from being fossil fuel based into one based on renewable energy requires the advent of more efficient and reliable energy storage media, both for transportation and to balance fluctuating clean energy sources such as wind and solar power. To this end, multiple technologies are currently under consideration, and secondary batteries are currently receiving a lot of attention, primarily due to the widely successful Li-ion battery.[1] For large scale storage applications, other battery types such as redox flow and metal air batteries also hold promise.[2–4]

The most successful metal air battery commercially is the primary Zn-air battery, widely used for small appliances that require a small amount of power for longer durations such as hearing aids. Zn-air batteries are attractive alternatives due to the benign chemistry and high theoretical specific energy of 1086 Wh kg^{-1}, much higher than Li-ion and only rivalled by few other chemistries such as Li-air,[5–8] The theoretical specific energy includes only the weight of Zn and the theoretical voltage. For practical purposes the specific energy attainable in a typical Zn-air hearing aid battery is currently 350-500 Wh kg^{-1},[9] which is approximately double of what is currently possible with Li-ion technology. For a secondary Zn-air battery the specific energy is lower due to restrictions on the level of charge and discharge of the Zn electrode.[10] Rechargeable Zn-air batteries are especially promising for stationary storage of electricity due to the earth crust abundance and availability of Zn.[11]

In an alkaline Zn-air battery, reduction of oxygen to hydroxyl takes place at the cathode during discharge. The hydroxyl ions in the electrolyte then participate in the main reactions on the negative Zn electrode, which are:

$$Zn + 4OH^- \leftrightarrow Zn(OH) + 3OH^- + e^- \leftrightarrow Zn(OH)_2 + 2OH^- + 2e^- \quad (1)$$

$$Zn(OH)_2 + 2OH^- + 2e^- \leftrightarrow [Zn(OH)_3]^- + OH^- + 2e^- \leftrightarrow [Zn(OH)_4]^{2-} + 2e^- \quad (2)$$

The first two OH adsorption steps (equation (1)) are electrochemical formation of zinc hydroxide ($Zn(OH)_2$), whereas the last two steps (equation (2)) are chemical formation of zincate ions ($[Zn(OH)_4]^{2-}$) in solution.[12] However, the dissolution of Zn starts already at $[Zn(OH)_3]^-$.[13] The zincate precipitates above its solubility limit to ZnO:

$$Zn(OH)_4^{2-} \leftrightarrow ZnO + H_2O + 2OH^- \quad (3)$$

The overall reaction is:

$$Zn + 2OH^- \leftrightarrow ZnO + H_2O + 2e^- \quad (4)$$

Secondary Zn-air batteries face various challenges that arise from cycling the battery, including:

- Dendrite formation;[14] as the zincate goes into solution it has no connection to the Zn electrode and is therefore free to adhere anywhere on the conducting electrode during charge. This can lead to dendrite formation, which in the worst case after some cycles can short circuit the battery.
- Bifunctional cathode;[6,15,16] since the positive electrode should reduce and evolve oxygen during discharge and charge respectively, a catalyst for both reactions needs to be employed (Bi-functional catalyst). As an alternative, two separate electrodes could be used, but that would complicate the battery cell design and reduce the specific energy.
- Precipitation of K_2CO_3 in the cathode as a side-effect of the alkaline electrolyte
- Flooding of the cathode if the hydrophobic properties of the cathode is not retained[17]
- Corrosion by hydrogen evolution

Hydrogen evolution follows this overall chemical reaction:

$$Zn + 2H_2O \rightarrow Zn(OH)_2 + H_2(g) \quad (5)$$

Here, the active material, Zn, is thus consumed without any electrons being transferred and $Zn(OH)_2$ is left.

As corrosion is also an issue in primary Zn-air batteries, it was previously alleviated by addition of Hg to the Zn.[18] Legislation has now limited the use of Hg in batteries due to its toxicity so other additives have been sought. At present, the negative electrode material in state-of-the-art primary Zn-air batteries consists of Zn with ppm doping levels of In, Bi and Al.[19] The effect of these additives over long term cycling is, however, poorly understood. Here follows a brief survey of the published effects of the doping elements and possible pollutants investigated in this work. Indium: The In-Zn phase diagram [20] shows a very small solubility of In in Zn, i.e. no mixing occurs except some solid solubility in mixtures with up to 0.2% In. Using Ni-In additives showed an apparent decrease in both HER and dendrite formation.[21] In ref. [22] Indium is shown to segregate to grain boundaries of Zn and decrease HER. Bismuth: Bi is also used in Zn electrode alloys (always in conjunction with another element though) in low doping concentration. The Bi-Zn phase diagram shows a very small solubility of 0.1% of Bi in Zn.[23] Bi is used as binder of particulate zinc to improve conductivity of zinc particles.[24,25] Plate-like Zn precipitates are found in Sn_8Zn_3Bi solder,[26] thus it seems Bi does not have any positive effect on dendrite formation. McBreen et al.[27] reports that a metallic Bi matrix (used together with $Ca(OH)_2$ in ref [28]) is responsible for increasing the cycle lifetime of a Zn electrode. Indium+bismuth: Yano et al.[29] report a surface alloy of In and Bi to be responsible for suppressing HER on the same level as a Hg additive. Many patents already exist for different mixtures of In and Bi with Zn for use in primary batteries. They are primarily for use in Zn electrodes in alkaline electrochemical cells or paint.[19,30–32] The materials in these patents can include dopant levels of the following elements as well: Pb, Al, Ga, Cd, Li, Ca, Fe and Mg. Although In and Bi are the most important additives, the other elements can play an important role as well if they have an preference for interacting with the active kink site for Zn dissolution,[12] as these sites can be infrequent on the zinc surface. Zn powders by Umicore, that are used for Zn electrode paste, contain approximately 100 ppm of the elements Bi, In and Al[1]. Silver: Ag in the negative Zn electrode is known

[1] The contents of "Zn BIA100" is from the chemical analysis in a Umicore - Certificate of Analysis obtained during the purchase of the powder.

to be responsible for greatly increasing hydrogen evolution, eventually making the battery effectively useless. Ag/Co_3O_4 is a promising catalyst for both the oxygen reduction reaction (ORR) and the oxygen evolution reaction (OER),[33,34] thus perfectly suited for Zn-air. For this reason, we have included Ag in this study since it may be transferred from the cathode catalyst through the electrolyte to the anode and thereby influence the electrochemical reactions.

In this paper, we systematically investigate the possible effects of In, Bi and Ag in a secondary Zn-air battery, focusing specifically on the behavior of the doping element on battery cycling and the effect of the dopant on especially the Zn dissolution and the HER. First, we will investigate the dissolution reaction on pure Zn surfaces with DFT and compare with previous work to establish that our method works. Next, we perform segregation studies to analyze how the surface is affected by different doping elements. Only elements that will stay in the surface during battery cycling will retain their effect in a secondary battery. We follow this by experimentally measuring the charge and discharge behavior of batteries with the theoretically determined additives on the negative electrode and quantifying the evolution of H_2 and O_2 with DEMS. Subsequently we use DFT to model adsorption of hydroxyl (OH) and hydrogen (H) to investigate Zn dissolution and hydrogen evolution reactions (HER), respectively on doped Zn electrodes. Since both reactions (equations (1) and (5)) involve the formation of $Zn(OH)_2$, we compare the affinity of the Zn surface to both OH and H to evaluate which reaction is preferred and thereby explain why some additives inhibit and others enhance HER. Thus, by studying the doped Zn electrode with a combination of DFT calculations and DEMS measurements, we can pinpoint the effect of the doping elements and determine if the effect is retained upon cycling.

Results and discussion

DFT study of zinc dissolution

Evaluating the free energy of electrochemical reactions with DFT within the framework of the computational hydrogen electrode approach[35] requires a few assumptions regarding the aqueous environment that is not explicitly calculated. This has been introduced and thoroughly covered previously and here follows only an overview that covers the terms needed for Zn surfaces with OH adsorbates.[12] Water is the source of OH in aqueous electrochemistry, thus the OH adsorption energy, ΔE, is calculated from the reaction: $H_2O + * \rightarrow OH* + H^+ + e^-$, where * denotes a free surface site and OH* is hydroxyl adsorbed on that site. The change in zero-point energy (ΔZPE) and entropy (ΔS) can be estimated from the reaction by vibrational mode analysis. The term ΔZPE – TΔS is estimated to be 0.39eV per OH at 298.15K.[12] Additionally, the aqueous environment stabilizes adsorbed species on the surface due to hydrogen bonding, ΔE_{aq}, which has previously been determined to 0.57eV per adsorbed OH molecule.[12] The applied potential is accounted for by adjusting the free energy by -neU, where n is the number of electrons transferred to the electrode, e is the electronic charge and U is the applied electrode bias. For reactions in solutions with pH different from 0, the free energy is corrected by $-kT \times \ln[H+] = kT \times \ln 10 \times pH$, where k is Boltzmann's constant and T is the temperature. The Zn-air system investigated here uses an alkaline electrolyte, thus we use a pH of 14. In total, the adsorption free energy of one OH molecule is calculated by:

$$\Delta G_{ads} = \Delta E - \Delta E_{aq} + \Delta ZPE - T\Delta S - kT \times \ln 10 \times pH - neU \quad (6)$$

The structures used for modelling the reactions are described in the method section. The surface is comprised of kink terminated steps separated by (0001) terraces. It is important to note that thermodynamically, a Zn atom prefers to be in the highest possible coordination. Thus, a real surface would be comprised of larger terraces with a much lower concentration of steps/kinks than those that are feasible to represent in a DFT simulations.

DFT-level modelling of the Zn electrode has only been reported to a limited degree in the literature. The starting point of the current investigation is the DFT study by Siahrostami et al.[12], where the dissolution reaction of undoped Zn in alkaline solution is found to proceed by dissolving the Zn surface by sequential removal of the residual kink atom on the edge. This mechanism exhibits a low overpotential and has no thermodynamic energy barrier since the dissolved kink atom leaves behind a new kink atom i.e. an unchanged surface. This is in contrast with the most stable surface; the Zn (0001) terrace, where a dissolved atom leaves behind a surface vacancy, which entails an energy barrier. The same holds if a Zn atom in the middle of a step edge is dissolved. This and the fact that undercoordinated sites typically are much more reactive [36] results in the kink-pathway to be the most probable for Zn dissolution. As illustrated by the atomic structures in Figure 1a, the mechanism starts with an OH molecule adsorbed at a bridge site between the two most undercoordinated Zn atoms (6- and 7-fold coordinated respectively) on the edge. As more OH molecules adsorb, the Zn atom at the kink is loosened and finally released as $[Zn(OH)_3]^-$.

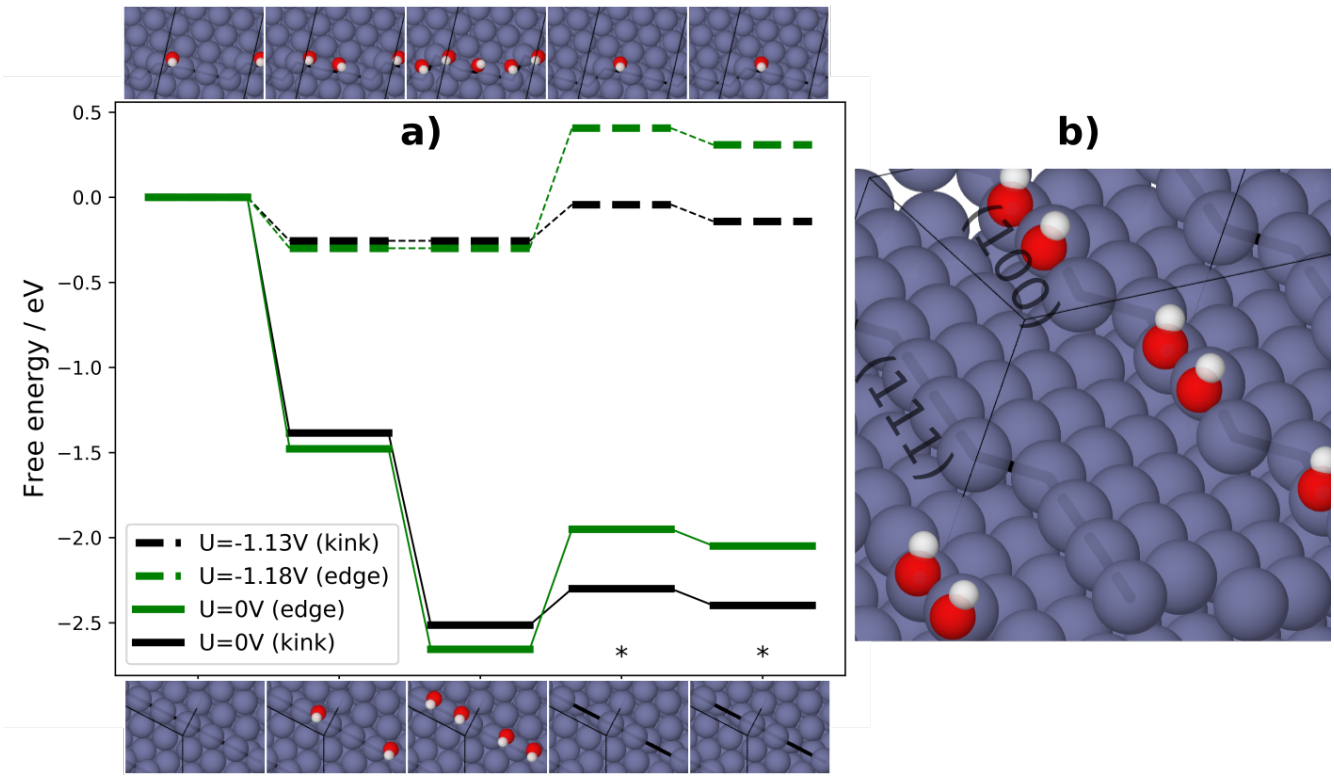

*Figure 1. a) The free energy diagram of the Zn dissolution reaction. Black and green lines represent kink and edge site dissolution respectively. The dashed lines show the energies when applying the limiting potentials as noted in the legend. The steps marked by * indicates that the energy is taken from experimental dissolution potentials. Above and below the graph are illustrations of the atomic structures from a top view at each step of the reactions dissolving a kink and edge Zn atom, respectively. Zn are grey, O red and H white. b) Side view of the second step in the reaction involving kink atom dissolution. The two types of microfacets (111) and (100)* [37] *are indicated.*

The graph in Figure 1a shows the free energy diagram for Zn dissolution with the reaction mechanism going through the kink and edge site on a pure Zn surface. The reaction mechanism is depicted in the illustrations above and below the free energy diagram for the reaction at the kink and edge sites, respectively. The first two steps are equation (1) and the last two are equation (2). Dissolved species are not well reproduced with DFT and the final two energy levels are therefore fixed to experimental dissolution potentials of $[Zn(OH)_3]^-$ and $[Zn(OH)_4]^{2-}$, respectively. These are -1.15V and -1.199V at pH 14.[38] The binding of OH is on average 0.1 eV stronger on the (100) microfacet compared to the (111) microfacet (see Figure 1b), thus all reported binding energies are from that step. The full lines represent the reactions with no applied bias, whereas the dashed lines are the free energy levels with the limiting potential applied. When a potential is applied, the free energy levels are corrected by the right-most term

in (6). The limiting potential is defined as the highest potential, where no electrochemical steps are uphill in free energy; if the limiting potential is smaller than the equilibrium potential there is an overpotential. The kink site dissolution has a limiting potential of -1.13V, very close to the value obtained in ref [12], and leading to an overpotential of 0.07V very close to 0.1V, which is the experimentally measured overpotential for pure Zn.[39]

For comparison, the Zn dissolution reaction for edge sites is also shown in Figure 1. It has a very similar limiting potential, but that reaction requires an edge vacancy to be formed. We have determined the cost of forming an edge vacancy to 0.35 eV, by using bulk Zn as a reference. This energy cost is added to the steps in which a Zn atom, in the form of $[Zn(OH)_3]^-$ or $[Zn(OH)_4]^{2-}$ has left the surface, marked with * on Figure 1a. This represents a chemical energy barrier for the mechanism removing an edge atom that is not present when removing the kink atom. The reason for clarifying the reaction mechanism on the edge will become evident when studying doped Zn, especially in the case of doping with Bi.

DFT study on arrangement of doping elements

To elucidate which elements could have a positive effect in secondary Zn-air batteries, by being thermodynamically stable in the surface of Zn both with and without an OH coverage, we have performed a segregation study of a series of elements on Zn; this is included in figure S3 of the supporting information. The three elements we will include in this study are In and Bi, which have a clear preference for the surface and has previously been shown to have beneficial effects for the negative Zn electrode, and Ag that has no clear surface preference but is known to have a disadvantageous effect on the Zn electrode. The preferential surface segregation of In and Bi means that the concentration in the surface of these elements will be larger than the ppm levels reported as optimal for powders.

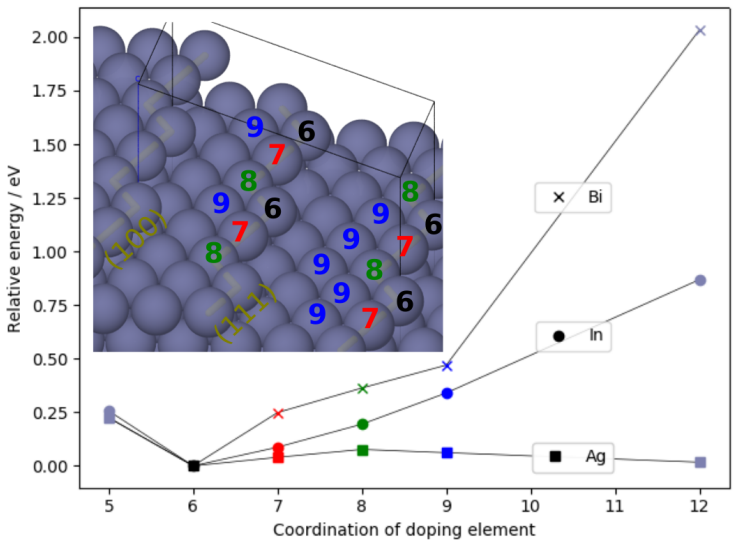

Figure 2. Relative energies of sites with different coordination of the dopant elements In, Bi and Ag. The energy of the dopants at sites with coordination number 6 (kink site) is defined as zero. The inset is an illustration of the kink structure. The numbers on the atoms indicate the coordination number of that atom. Coordination 6: Kink site atom, 7: edge atom, 8: edge atom just behind a kink and 9: atom in the terrace. Not shown are sites on the surface (coordination 3-5) and below the surface (coordination 10-12) which were all higher in energy. Indicated are also the two types of step microfacet ((100) and (111)) present in the computational cell.

Figure 2 shows the relative energy for different placements of a single atom of In, Bi and Ag on the kinked Zn surface without considering any adsorbate effect. Since the computational cell contains two steps, the (100) and (111) microfacets which has not been considered previously, the relative energy in the figure is an average of dopant placements at or near each step. The energy as a function of coordination follows the same trend at both steps. The kink site is the most favorable site for In and Bi to reside. For In, the 7-fold coordinated step site lies very close in energy, whereas for Bi all other coordination types are related to large energy penalties. Sites with low coordination, like adatoms on a terrace (coordination number 3), were also tested and found to be unfavorable. This means that the mechanism for Zn dissolution proposed for pure Zn in ref [12] will not proceed exactly as described the doped systems, because the active site in that process will change with In or Bi additives. The favored site of Ag is not as clearly established. The energy gain for a 6-fold coordinated Ag, at the kink site, is less than 0.1 eV compared to the other surface sites. Compared to a 12-fold coordinated bulk site the

energy gain is even less. Thus, it is improbable that Ag will stay in the surface of Zn during recycling of a secondary battery. The risk of having Ag on the negative Zn electrode is, however, still present during cycling in a secondary Zn-air battery if it is used in combination with an unstable catalyst for the air-electrode, e.g. Ag/Co_3O_4Thus, the effect of the element is still important to analyze. With these findings, we proceed with our experimental investigations to show that the additives influence charge/discharge voltages and investigate the influence on the performance during cycling with In, Bi and Ag additives. We will revisit the dissolution reactions for doped Zn surfaces with DFT afterwards.

DEMS study on anode cycling with dopants

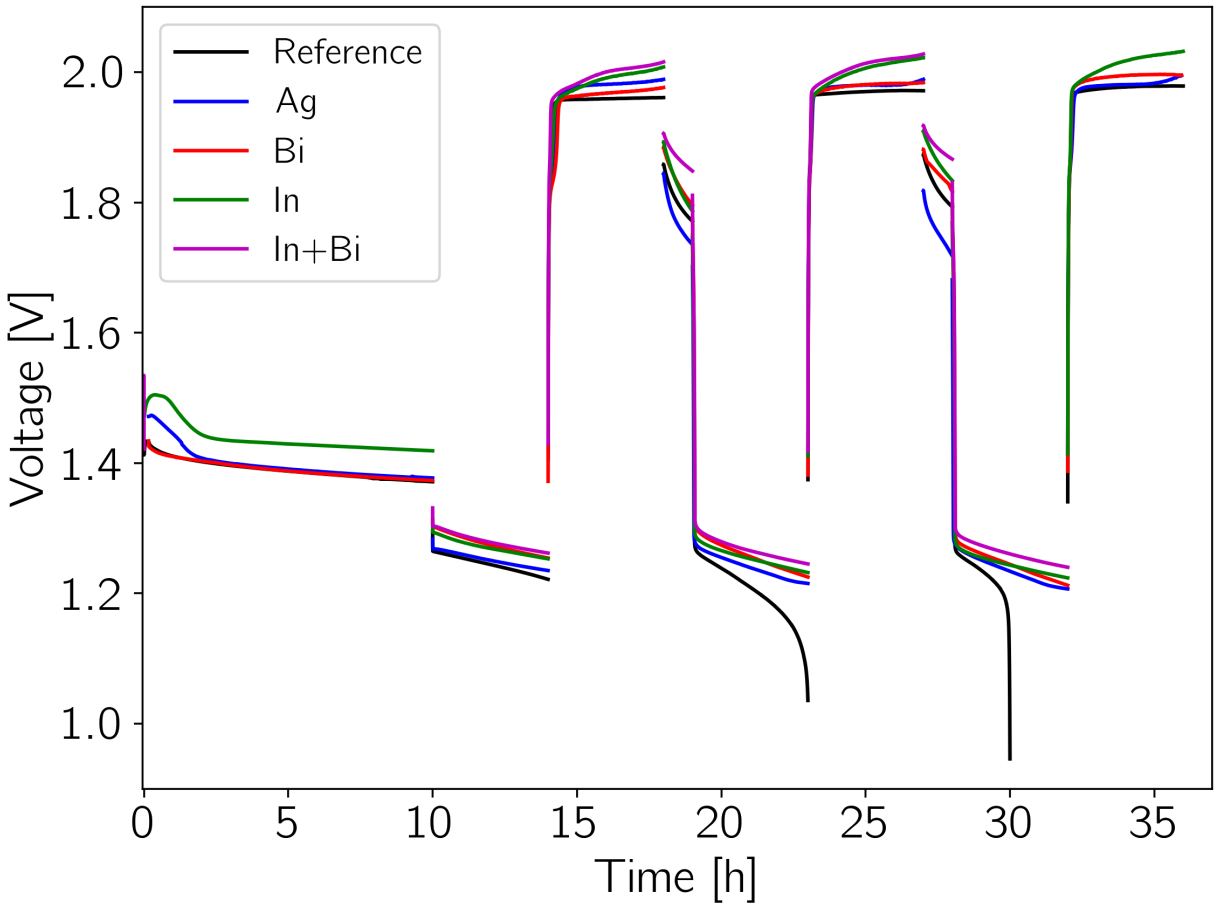

Figure 3. Galvanostatic cycling data consisting of discharge-charge cycles at 1 mA/cm^2 for five Zn-air batteries with a Zn foil anode and a $NiCo_2O_4$ cathode. One reference battery (black) and four batteries with additives Ag (blue), Bi (red), In (green) and a 50:50 mixture of In and Bi (purple) in the electrolyte were measured. Each discharge and charge were limited to 4 hours. The open circuit voltage (OCV) was measured for 10 hours before the first cycle and for 1 hour before the second and third discharge.

The galvanostatic cycling data in Figure 3 show the electrochemical behavior of a reference Zn-air battery and four similar batteries each with a different additive. Common features across all the measurements are that the initial OCV (open circuit voltage) decreases and that the first discharge plateau has a slight slope. See figure S1 for an analysis of the slope for the different additives. Care should be taken when evaluating very small differences in the experimentally determined overpotential as contributions from e.g. contact resistance could influence the absolute value of the measured voltage. During charge, the reference Zn-air battery exhibits a flat charge plateau at 1.95 V, while the cells with additives are slightly higher and increases with charge time. Particularly the cells containing In additive show increasing charging potential over time. After the first charge, the OCV value is around 1.8 V. The increase in OCV compared to the pristine cell is due to a slight oxidation of the cathode. During the second discharge, the reference Zn-air cell potential shows a drastic decline until the discharge time limit. During the third charge, this feature is even more significant with the potential reaching the lower potential limit of 0.95 V. Despite this, the charge proceeds for the full duration of 4 hours for both the second and third charge. This is a result of non-electrochemical reactions taking place during discharge (chemical oxidation and hydrogen evolution) and/or oxidation of other species (e.g. in the catalyst) taking place during charge.

The discharge potentials decrease with each cycle for all additives, see figure S1 in the supporting information. The Ag additive results in decreasing charge potential with each cycle, indicating that the effect of Ag diminishes over cycling. The charging potentials of the other additives increase slightly but their relative differences remain stable. The addition of In to the electrolyte is beneficial, resulting in higher OCV and discharge potential although during charge the overpotential is increased. Although this does not initially appear to be beneficial, it is related to a suppression of parasitic reactions as discussed below. Bi has a similar low overpotential on discharge, but it increases with more cycles. On charge, the

voltage is constant with a slightly higher overpotential than the reference Zn sample. The combination of In and Bi consistently has the highest OCV and discharge potentials. The same is true for charge potentials but, as with In, the effect of suppressing parasitic reactions outweigh the detrimental effect on energy efficiency.

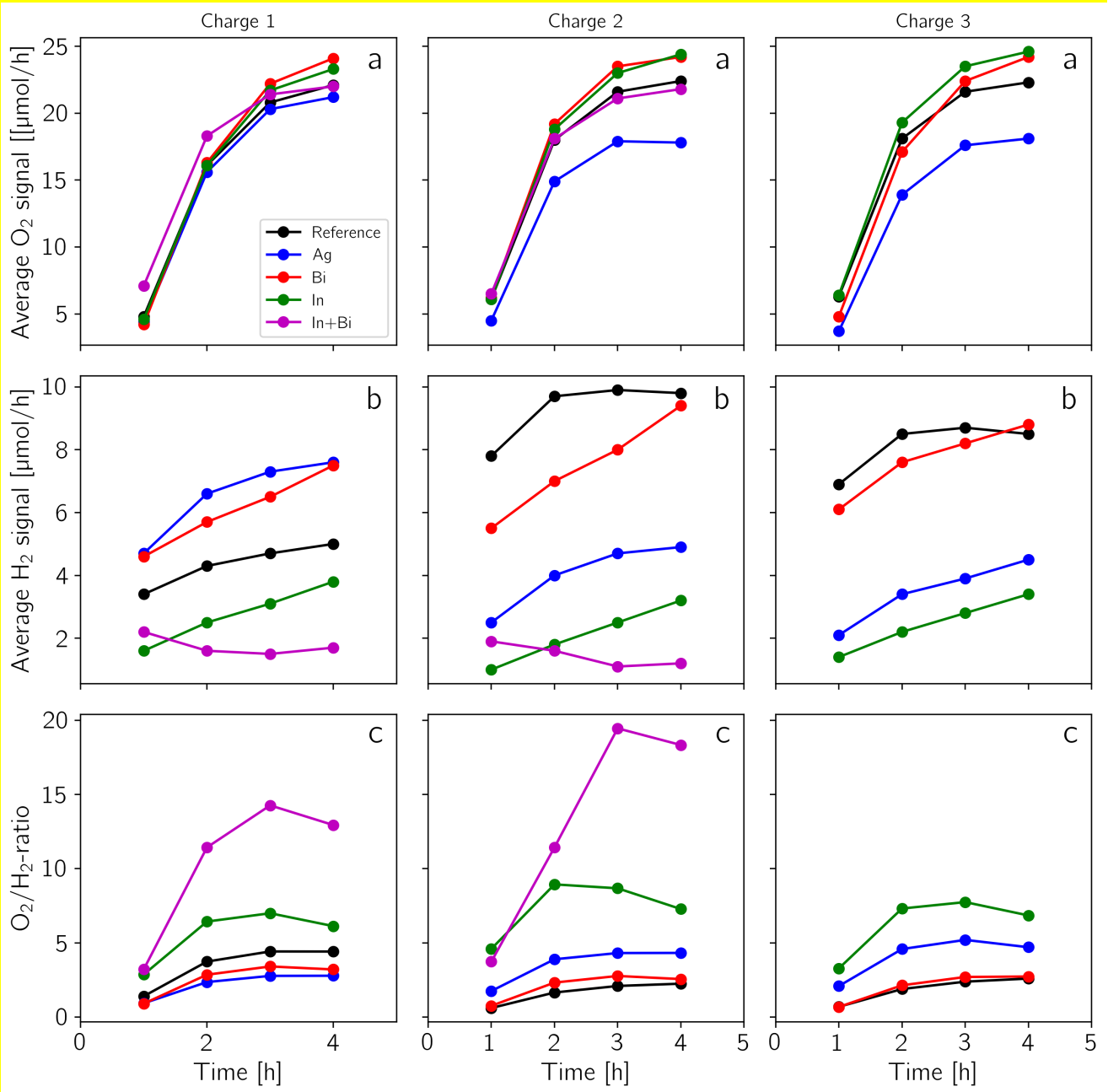

Figure 4. DEMS data collected during charge for each cell. Mass spectrometer data were collected every 10 minutes from the headspace of the cell and were averaged to obtain hourly gas production rate (µmol/h). Row a) the hourly average O_2-signal, row b) the hourly average H_2-signal, row c)the respective O_2/H_2 ratio.

From the DEMS measurements it is possible to quantify the amount of hydrogen and oxygen evolved and to correlate this with the number of electrons passed through the cell. This allows determination of the efficiency of the electrochemical processes (e.g. determining the number of electrons per oxygen evolved) and to detect parasitic reactions. In this work the DEMS measurements were used to quantify the electrochemical oxygen evolution and determine the contribution from electrochemical and chemical hydrogen production. As mentioned earlier, the electrochemical hydrogen production is from water splitting, while the chemical hydrogen evolution is from chemical oxidation of zinc metal.

In Figure 4, the effect of the additives on OER and HER during charge is broken down into hourly production. The low initial signal during each charge is due to the large headspace of the electrochemical cell used, which creates a delay in detection of the gasses evolved. On the first cycle, the O_2 signals are similar between the reference and the cell with Ag additive, but the Ag additive yields more H_2. With increased cycle number, the H_2 signal decreases along with the O_2 signal. The decreased H_2 signal with cycling is consistent with the DFT study on the additive arrangement, see Figure 2, which suggests that Ag is not preferred on the surface of Zn, also see figure S2 and table 1 in the supporting information for the exact DEMS signals. In the case of an Ag-containing air electrode like Ag/Co_2O_3), additional Ag may shuttle to the Zn electrode, unless an Ag-separator is used, resulting in enhanced H_2-evolution. The data supports the theoretical findings that Bi primarily affects the potentials of the Zn-air battery as the H_2 and O_2 production levels are nearly identical to the reference with Bi slightly promoting O_2. Adding In is beneficial as it, similarly to Bi, promotes O_2 evolution while simultaneously decreasing the H_2 evolution. During charging, the battery with In additives has a different charging profile with higher potential and higher slope than batteries with pure Zn or other additives. It is, however, important to note that at the same time the H_2-evolution is dramatically decreased compared to all the batteries without In additives, showing that the suppression of parasitic hydrogen evolution increases with time and with the number of cycles. It indicates that a more efficient distribution of In on the Zn surface is established during cycling.

When Bi and In are added together, the O_2 evolution is similar to the other additives and the H_2 evolution is at its lowest in all the experiment, while still maintaining the highest discharge potential (see Figure 3) and sustaining the positive effects over cycling. As such, the In+Bi additives dramatically affect the conditions and performance of the Zn electrode. By examining the ratio of O_2 to H_2, it is clear that Ag is not a desirable additive and while a similar statement could be made for Bi, the DEMS data suggest that the beneficial effect of Bi is primarily from the stabilization of the discharge potentials as seen on figure S1 in the supporting information as well as further suppression of H_2 evolution when combined with In. In summary, adding In is clearly beneficial despite the increased overpotential on charging, that would lower the apparent energy efficiency, but due to the lowered H_2 evolution there is less degradation of the Zn electrode, thus improving cycle life. Mixing In and Bi combines the beneficial properties of each additive as it yields the best O_2 to H_2 ratio, better than In by itself and also yields high discharge potentials. In order to gain a better understanding of the synergy and gain further insights on the mechanistics of the In and Bi additives, we have performed additional DFT calculations on the Zn dissolution reaction mechanism on the doped systems.

DFT study on Zn dissolution with dopants

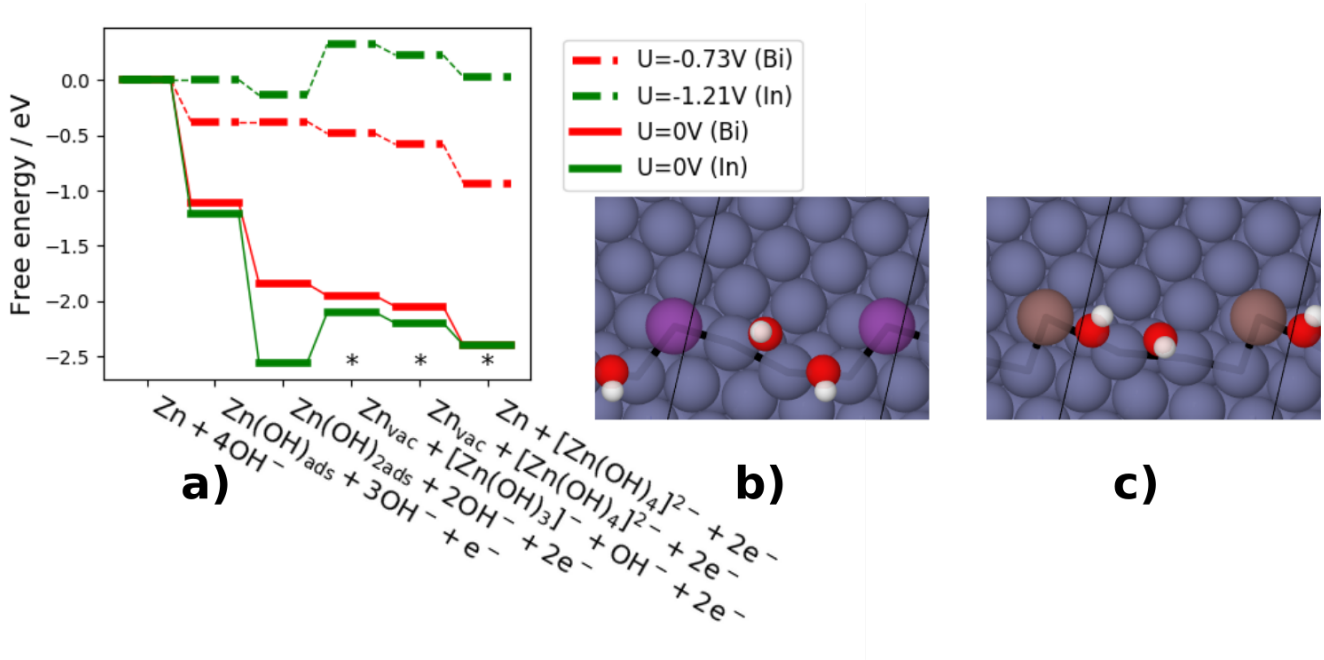

*Figure 5. a) Free energy diagram of the electrochemical steps of Zn dissolution on In and Bi doped Zn surfaces. Full and dashed lines are with no potential and the limiting potential applied respectively. * marks the energy levels fixed to experimental dissolution potentials. b) Atomic illustration of the second step in the reaction with Bi doping. c) as b) but with In doping.*

Doped with Bi and In, the free energy diagram for Zn dissolution takes the form as shown in Figure 5a. The dissolution of a Zn atom from the step leaves a vacancy whose energy is added to the third and second last steps in the free energy diagram, the final step rearranges the step on the surface and removes the vacancy. The last adsorption step of OH before the dissolution of $[Zn(OH)_3]^-$ on the Bi and In doped surfaces is shown in Figure 5b and c respectively; two OH molecules are adsorbed and the Zn atom about to dissolve coordinates to both molecules. The different effects of the two dopants are clearly visible; OH avoids the Bi atom situated at the kink site, thus an edge atom is dissolved instead. Here, it should be noted that the low limiting potential of -0.73 V shown in Figure 5a is an artifact of the limited size of the computational cell. For a more realistic kink to kink distance, there would not be an interaction between the leaving Zn atom and the doping element on the next kink (see Figure 5b), so the dissolution process would follow the edge mechanism, as shown in Figure 1a, leading to a limiting potential of approximately

-1.18 V. The vacancy cost used here is 0.35 eV, the same as estimated for the pure Zn edge. During the adsorption process, In is displaced a little from the kink site allowing OH to adsorb to the Zn atom closest to the kink; this atom dissolves from the step and the vacancy formation energy penalty in this reaction stems from In moving back to its favored position at the kink, which is determined to be 0.2 eV for the (100) microfacet. The calculated limiting potential for the In-doped system is -1.21 V. Since the equilibrium potential is -1.199 V In doping effectively removes the fundamental overpotential. This effect comes from the stronger binding of the OH closest to the Zn, due to a favorable interaction with In.

The addition of both In and Bi is found to stabilize the cyclic performance as shown in Figure 3. With DFT, we have determined that the combination of both elements at a step is in fact more stable than each step only having one of the two dopants. The energy gain by having two steps with Bi-In neighbors as an edge termination compared to one with In-In and one with Bi-Bi edge terminations is 0.1 eV/doping atom, i.e. a significant stabilization explaining the almost constant charge and discharge potentials for In+Bi in Figure 3.

Figure S4 in the supporting information shows the free energy diagram of Ag-doped Zn. The effect of Bi and Ag is very similar; adsorption of OH is weakened leading to the Zn dissolution reaction to involve Zn atoms on the edge. At this point, a question arises: if Ag and Bi apparently behave similarly, why is Ag detrimental for Zn-air batteries while Bi is used in the state of the art Zn paste? The answer is revealed when looking at adsorption (and in turn production) of hydrogen.

DFT study of corrosion vs dissolution

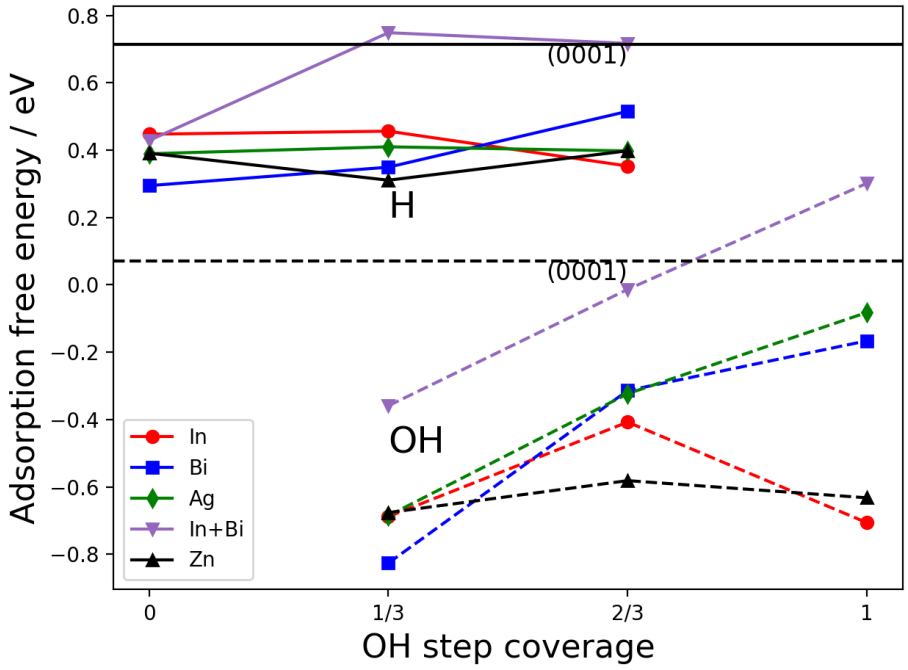

Figure 6. Comparison of binding energies of H and OH on kink surfaces either pure Zn or doped with In, Bi or Ag. The adsorption free energy of H and OH on the kink Zn surface with increasing amount of OH already adsorbed (coverage). Full and dashed lines are for H and OH adsorption, respectively. The horizontal lines spanning the whole x-axis represent adsorption energies on the (0001) terrace.

As discussed in the introduction, both Zn dissolution and hydrogen evolution reactions go through a $Zn(OH)_2$ intermediate, see equations (1) and (5). In Figure 6, we compare the adsorption energies of H and OH on both pure and doped Zn with an increasing coverage of OH, to determine how both reactions are influenced by dopants; a similar method has been used previously to compare CO_2 reduction and HER.[40] From the binding energies of OH in the bottom part of Figure 6 it is seen that, for both Bi and Ag, the energy gain by adsorbing OH decreases with respect to the pure Zn surface and thereby Zn dissolution is hampered. The adsorption energy curves for Bi and Ag are approaching the energy for terrace adsorption as the OH coverage increase, it is thus not unlikely that a too large concentration of Bi in the Zn electrode will block the edges completely and could drive Zn dissolution to take place on the terrace.

The adsorption energies of OH for the In-doped system has a bump at 2/3 coverage, but decreases with coverage; the same is seen for the adsorption of H. Thus, the reported decrease in HER in In-doped Zn,[22] also seen in Figure 4, must come from the fact that the decrease in adsorption energy of H is outweighed by the decrease in OH adsorption energy. Bi has the opposite effect on H adsorption, so although the effect of Bi is seemingly detrimental to Zn dissolution by lowering the OH affinity, it is also detrimental to HER. Overall, the presence of Bi therefore has a positive effect on the Zn electrode, in particular when co-doped with In. On the other hand, Ag does not exhibit the same weakening of H adsorption as Bi, so Ag only hampers Zn dissolution, leaving HER as the preferred process.

The combined In+Bi adsorption energies show a trend different from the other adsorbates. OH adsorption energies are markedly higher, but this can be explained by the limited number of sites available on the step; all dopant calculations have been performed on a constant sized step. With two doping atoms there is effectively one less site available for adsorption. Thus, by shifting the In+Bi OH line to the right by 1/3 coverage one achieves almost identical values to the Bi doping. This cannot account for the H adsorption behavior, since the increase in adsorption energy takes place already at an OH coverage of 1/3, where free sites with only Zn are available. The decrease must then come down to an electronic effect of the combined In and Bi. Only the combination of both In and Bi can switch the most favorable adsorption site for H to the (0001) terrace where HER is not considered an issue.[2] For all other dopants, the adsorption energy of H on Zn (0001) is still 0.2 eV higher than the highest energy on the kink.

Conclusion

The Zn dissolution and parasitic hydrogen evolution reaction at the negative electrode in secondary Zn-air batteries were modelled with DFT and measured experimentally with DEMS on In, Bi and Ag doped as well as pure Zn surfaces. To influence the negative electrode chemistry upon cycling of the battery, the doping elements need to be thermodynamically or kinetically stabilized in the surface as Zn is plated on the negative electrode during charge. DFT calculations showed that In and Bi strongly prefers to be

situated at the kink site, whereas there was no clear driving force for Ag to stay in the surface. This is also confirmed experimentally, where In and Bi changes the potential characteristics as well as O_2/H_2 evolution consistently through cycling, compared to pure Zn foil, and the effect of Ag is lost after a few cycles. Both DFT calculations and DEMS measurements show that In decreases the overpotential for Zn dissolution. The primary effect of Bi is found to be stabilizing In in the Zn-surface; DEMS measurements with both dopants shows a constant behavior of the charge/discharge potentials over cycling. The DFT calculations confirm that steps with both Bi and In are 0.1 eV/doping atom more stable than individual steps with only one of the doping element. The co-doping of both In and Bi was observed to decrease the HER dramatically as seen in Figure 4 and the decrease in HER was explained with DFT to stem from a much weaker H adsorption on Bi and In co-doped steps. In the same manner, Ag was found to increase the HER, demonstrating a weakening of the OH binding energy, but has no effect on H binding, leaving HER as the preferred reaction.

Method section

Computational details

The density functional theory calculations were all performed with GPAW (v0.11.0) code [41,42], which is a real space implementation of the PAW method.[43] Structure manipulation and post analysis of calculations where performed with ASE (v3.9.1).[44] The RPBE functional [45] has been employed, this functional was developed to provide accurate adsorption energies for molecules on surfaces. All reported energies are calculated with the finite difference (fd) mode in GPAW, working on the real space grid.

All geometrical relaxations of clean surfaces are performed in a two-step procedure, where the linear combination of atomic orbitals (LCAO) mode in GPAW [46] is used for the initial relaxation followed by a relaxation in fd mode. This allows the computationally cheaper LCAO mode to do the heavy lifting of the geometrical relaxation of the Zn surface that, due to its low surface energy, tend to require many relaxation steps. For calculations of adsorbed species, this approach was not found to be advantageous, thus a full relaxation in fd mode is performed. It is known that the basis set superposition error (BSSE),[47] present in LCAO mode calculations, artificially enhances the interaction between adsorbate and substrate. This could lead to incorrect geometries since the correction scheme is not applicable when extracting forces from GPAW calculations at the moment.

The free energy diagram of zinc dissolution is calculated from the adsorption energies using a well-known recipe[35] and also used on the previous DFT study on Zn dissolution.[12] We assume the temperature to be 298.15 K and the pH to be 14.

All adsorption energies, except the edge dissolution pathway illustrated in the lower part of Figure 1a, are reported from a structure with 4 atoms on each step in the unit cell, each step is terminated by a kink, which is a 6-fold coordinated atom. For a representative illustration see Figure 1b and the inset in Figure 2. As previously mentioned, the computational cell contains two steps with microfacets of the types (100)

and (111). If not stated otherwise the reported energies stem from adsorption on the (100) step, as these are all more stable. To avoid interaction between steps they are separated by 3 and 4 terrace rows. The interaction between a kink atom and its periodic image is minimal. The unit cell has 4 close-packed Zn atomic layers, during geometrical relaxation the bottom two are fixed to the bulk structure and lattice constant. We use the experimental lattice constant of a = 2.66 Å, c = 4.94 Å.[48] Perpendicular to the surface a vacuum of 12 Å is inserted to prevent interaction between computational slabs. We use a (3, 3, 1) k-point sampling in a Monkhorst-Pack scheme[49] and a grid spacing of 0.18 Å.

DEMS measurements

All electrochemical measurements were performed using a 2 electrode ECC-Air-Ni cell from EL-Cell. The cathode was $NiCo_2O_4$ (NCO) with PTFE for hydrophobicity and µm Ni particles for conductivity supported on Ni 40 mesh. The electrolyte was 200 µL 6 M KOH and contained two 260 µm thick GF/A Whatman glass fiber separators. The additives Ag, Bi and In were added from 0.005 M Ag/Bi/In-nitrate solution. Additionally, an additive with 0.0025 M In- and 0.0025 Bi-nitrate was added to a zinc-air cell. The metal nitrate salts were acquired from Sigma Aldrich of at least 99.9% pure and the concentrations were calculated from the anhydrous weight. The Bi-nitrate which is not completely soluble in water was sonicated and stirred before use to ensure that the particles were dispersed well in solution. 28 µL of the additive solution were added to the cell between the two separators before electrolyte was added. The current collector for the positive electrode was a Ni perforated plate from EL-Cell. The current collector for the negative electrode was 8 µm thick 99.99% Cu-foil from MTI corp.

Experimental Procedure

Each cell was cycled 3 times with OCV-measurements prior each discharge-charge. The Initial OCV time was 10 hours while the flowing OCV-measurement time is 1 hour. The galvanostatic cycling was four hours at a current of 1 mA/cm^2 (geometric area) for both discharge and charge. DEMS measurements were performed during charging with the setup as described in.[50–52] The gas was collected every 10

minutes. After each discharge the cell is flushed for an hour to remove oxygen in the headspace of the cell.

Anode preparation

Zn foil electrodes were stamped from a 99.95% purity 0.125mm thick Zn sheet (Goodfellow). After stamping the foil were washed in purified water and alcohol to remove residue.

Cathode preparation

The $NiCo_2O_2$ (NCO) cathodes were made from 39 wt% $NiCo_2O_4$ powder (Cerpotech), 23 wt% 3-7 μm Ni powder, 23 wt% 150-200 mesh Ni powder (Strem Chemicals) and 15 wt% PTFE (Sigma Aldrich) onto Ni 40 mesh (Alfa Aesar) total loading of 157±25/cm^2 g. The powders are mixed, compressed and heated at 340 °C for 1 hour.[28]

Acknowledgements

This work was supported by the Horizon 2020 framework project ZAS, grant number 646186. We would also like to acknowledge Prof. Peter Holtappels and Dr. Vladimir Tripkovic for valuable discussions. Furthermore, Dr. Alexander Kube is acknowledged for providing the $NiCo_2O_4$ catalyst.

Keywords

- Density functional theory calculations
- Differential Electrochemical Mass Spectrometry
- Secondary Zinc-air batteries
- Doping
- Electrochemistry

References

[1] V. Caramia, B. Bozzini, *Mater. Renew. Sustain. Energy* **2014**, *3*, 28.

[2] P. Gu, M. Zheng, Q. Zhao, X. Xiao, H. Xue, H. Pang, *J. Mater. Chem. A* **2017**, *5*, 7651–7666.

[3] M. A. Rahman, X. Wang, C. Wen, *J. Electrochem. Soc.* **2013**, *160*, A1759–A1771.

[4] J. Fu, Z. P. Cano, M. G. Park, A. Yu, M. Fowler, Z. Chen, *Adv. Mater.* **2017**, *29*, 1604685.

[5] Y. Li, H. Dai, *Chem. Soc. Rev.* **2014**, *43*, 5257–75.

[6] E. Davari, D. Ivey, *Sustain. Energy Fuels* **2017**, *2*, 39–67.

[7] K. G. Gallagher, S. Goebel, T. Greszler, M. Mathias, W. Oelerich, D. Eroglu, V. Srinivasan, *Energy Environ. Sci.* **2014**, *7*, 1555.

[8] T. Vegge, J. M. Garcia-Lastra, D. J. Siegel, *Curr. Opin. Electrochem.* **2017**, *6*, 100–107.

[9] Y. Li, J. Lu, *ACS Energy Lett.* **2017**, *2*, 1370–1377.

[10] O. Haas, J. Van Wesemael, *Encyclopedia of Electrochemical Power Sources*, Elsevier, **2009**.

[11] P. C. K. Vesborg, T. F. Jaramillo, *RSC Adv.* **2012**, *2*, 7933.

[12] S. Siahrostami, V. Tripković, K. T. Lundgaard, K. E. Jensen, H. A. Hansen, J. S. Hummelshøj, J. S. G. Mýrdal, T. Vegge, J. K. Nørskov, J. Rossmeisl, *Phys. Chem. Chem. Phys.* **2013**, *15*, 6416–21.

[13] Y.-C. Chang, G. Prentice, *J. Electrochem. Soc.* **1984**, *131*, 1465.

[14] A. L. Zhu, D. P. Wilkinson, X. Zhang, Y. Xing, A. G. Rozhin, S. A. Kulinich, *J. Energy Storage* **2016**, *8*, 35–50.

[15] V. Tripkovic, H. A. Hansen, T. Vegge, *ChemSusChem* **2018**, *11*, 629–637.

[16] V. Tripkovic, H. A. Hansen, T. Vegge, *ACS Catal.* **2017**, *7*, 8558–8571.

[17] D. Schröder, T. Arlt, U. Krewer, I. Manke, *Electrochem. commun.* **2014**, *40*, 88–91.

[18] L. M. Baugh, F. L. Tye, N. C. White, *J. Appl. Electrochem.* **1983**, *13*, 623–635.

[19] I. A. J. Strauven, M. L. Meeus, *Zinc Powder for Alkaline Batteries - Patent CA2153330 A1*, **1994**.

[20] J. Dutkiewicz, W. Zakulski, *Bull. Alloy Phase Diagrams* **1984**, *5*, 284–289.

[21] C. W. Lee, K. Sathiyanarayanan, S. W. Eom, H. S. Kim, M. S. Yun, *J. Power Sources* **2006**, *159*, 1474–1477.

[22] A. G. Muñoz, S. B. Saidman, J. B. Bessone, *Corros. Sci.* **2001**, *43*, 1245–1265.

[23] J. Vizdal, M. H. Braga, A. Kroupa, K. W. Richter, D. Soares, L. F. Malheiros, J. Ferreira, *Calphad Comput. Coupling Phase Diagrams Thermochem.* **2007**, *31*, 438–448.

[24] L. Lin, R. Shepard, *United States Patent 6,300,011 B1*, **2001**.

[25] R. E. Durkot, L. Lin, P. B. Harris, *United States Patent 6,284,410 B1*, **2001**.

[26] M. Y. Chiu, S. S. Wang, T. H. Chuang, *J. Electron. Mater.* **2002**, *31*, 494–499.

[27] J. McBreen, E. Gannon, *J. Power Sources* **1985**, *15*, 169–177.

[28] C. Zhang, J. M. Wang, L. Zhang, J. Q. Zhang, C. N. Cao, *J. Appl. Electrochem.* **2001**, *31*, 1049–1054.

[29] M. Yano, S. Fujitani, K. Nishio, Y. Akai, M. Kurimura, *J. Power Sources* **1998**, *74*, 129–134.

[30] C. Henninot, Y. Strauven, *Methods for Manufacturing Alloyed Zinc Powders with Pierced Particles for Alkaline Batteries - United States Patent 2012/0096989 A1*, **2012**.

[31] K. Kuwayama, J. Nakagawa, K. Tomii, K. Hagimori, *Zinc Alloy for Use with Electrode - United States Patent 4,432,937*, **1984**.

[32] H. W. Sarkas, I. V Barsukov, *Zinc Anode Alkaline Electrochemical Cells Containing Bismuth - United States Patent 9105923 B2*, **2015**.

[33] R. Gao, Z. Yang, L. Zheng, L. Gu, L. Liu, Y. L. Lee, Z. Hu, X. Liu, *ACS Catal.* **2018**, acscatal.7b03566.

[34] D. Wittmaier, N. A. Cañas, I. Biswas, K. A. Friedrich, *Adv. Energy Mater.* **2015**, *5*, 1–8.

[35] J. K. Nørskov, J. Rossmeisl, A. Logadottir, L. Lindqvist, J. R. Kitchin, T. Bligaard, H. Jónsson, *J. Phys. Chem. B* **2004**, *108*, 17886–17892.

[36] S. H. Brodersen, U. Grønbjerg, B. Hvolbæk, J. Schiøtz, *J. Catal.* **2011**, *284*, 34–41.

[37] M. A. Van Hove, G. A. Somorjai, *Surf. Sci.* **1980**, *92*, 489–518.

[38] M. Cai, S.-M. Park, *J. Electrochem. Soc.* **1996**, *143*, 2125.

[39] J. C. Salas-Morales, J. W. Evans, *J. Appl. Electrochem.* **1994**, *24*, 858–862.

[40] Y.-J. Zhang, V. Sethuraman, R. Michalsky, A. A. Peterson, *ACS Catal.* **2014**, *4*, 3742–3748.

[41] J. J. Mortensen, L. B. Hansen, K. W. Jacobsen, *Phys. Rev. B* **2005**, *71*, 35109–35111.

[42] J. Enkovaara, C. Rostgaard, J. J. Mortensen, J. Chen, M. Dulak, L. Ferrighi, J. Gavnholt, C. Glinsvad, V. Haikola, H. A. Hansen, et al., *J. Physics-Condensed Matter* **2010**, *22*, 253202.

[43] P. Blöchl, *Phys. Rev. B* **1994**, *50*, 17953–17979.

[44] A. Hjorth Larsen, J. J. Mortensen, J. Blomqvist, I. E. Castelli, R. Christensen, M. Dułak, J. Friis, M. N. Groves, B. Hammer, C. Hargus, et al., *J. Phys. Condens. Matter* **2017**, *29*, 273002.

[45] B. Hammer, L. Hansen, J. Nørskov, *Phys. Rev. B* **1999**, *59*, 7413–7421.

[46] A. H. Larsen, M. Vanin, J. J. Mortensen, K. S. Thygesen, K. W. Jacobsen, *Phys. Rev. B* **2009**, *80*, 195112.

[47] F. B. van Duijneveldt, J. G. C. M. van Duijneveldt-van de Rijdt, J. H. van Lenthe, *Chem. Rev.* **1994**, *94*, 1873–1885.

[48] N. W. Ashcroft, N. D. Mermin, *Solid State Physics*, Saunders, **1976**.

[49] H. J. Monkhorst, J. D. Pack, *Phys. Rev. B* **1976**, *13*, 5188–5192.

[50] J. Højberg, K. B. Knudsen, J. Hjelm, T. Vegge, *ECS Electrochem. Lett.* **2015**, *4*, A63–A66.

[51] J. Højberg, PhD Thesis: Fundamental Mechanisms in Li-Air Battery Electrochemistry, **2015**.

[52] J. Højberg, B. D. McCloskey, J. Hjelm, T. Vegge, K. Johansen, P. Norby, A. C. Luntz, *ACS Appl. Mater. Interfaces* **2015**, *7*, 4039–4047.

Entry for Table of contents

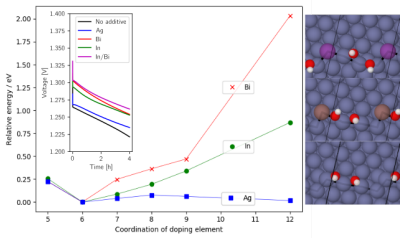

Changing the Zn dissolution reaction mechanism by doping: By combining density functional calculations with differential electrochemical mass spectrometry measurements it is established that In and Bi lower the overpotential on discharge, reduce H_2 evolution and increase the stability of the doped structure over battery cycling.